Austrian Journal of Earth Sciences | Vienna | 2016 | Volume 109/2 | 166 - 177 | DOI: 10.17738/ajes.2016.0012

Petrology and geochemistry of metabasalts from the Taoxinghu ophiolite, central Qiangtang, northern Tibet: Evidence for a continental back-arc basin system

Yan-wang WU[1) 2)], Cai LI[4)], Meng-jing XU[3) *)], Sheng-qing XIONG[1)], Zheng-guo FAN[1)], Chao-ming XIE[4)] & Ming WANG[4)]

[1)] China Aero Geophysical Survey & Remote Sensing Center for Land and Resources, Beijing 100083, China;

[2)] School of Geophysics and Information Technology, China University of Geoscience (Beijing), Beijing 100083, China;

[3)] School of Geology and Geomatics, Tianjin Chengjian University, Tianjin 300384, China;

[4)] College of Earth Science, Jilin University, Changchun 130061, China;

[*)] Corresponding author: mengjing_xu@126.com

KEYWORDS Qinghai-Tibet Plateau; Paleo-Tethys; central Qiangtang; SSZ-type ophiolite; geochemistry

Abstract

Newly discovered ophiolitic metabasalts in the Taoxinghu area of central Qiangtang on the Qinhai-Tibet Plateau, here described for the first time, have important implications for reconstructions of the tectonic history of the Paleo-Tethys Ocean. Most of the metabasalts belong to the tholeiitic basalt series and most have undergone greenschist-facies metamorphism. The distribution of rare earth elements and trace elements shows that the rocks are typical of sub-continental margin arc-basin lavas, similar to the environment of formation of the present-day Okinawa lava, suggesting that the Taoxinghu metabasalts represent the upper portions of a supra-subduction zone (SSZ)-type ophiolite that formed in a continental back-arc basin tectonic environment. The Taoxinghu metabasalts are mainly sourced from a depleted spinel mantle-source region, with a spinel lherzolite content equivalent to partial melting of 6 %-25 %. In addition, lava compositions were likely affected by melting of sediments during subduction, while the influence of aqueous fluids was minor. Combining with the existing knowledge on the ophiolites of Longmuco-Shuanghu-Lancang suture zone (LSLSZ), an evolutionary model is proposed. The LSLSZ Paleo-Tethys Ocean basin may have started to form during the Cambrian or earlier, and subducted in the early Carboniferous. As subduction proceeded, a continental back-arc basin was developed, the site of generation of most of the Taoxinghu metabasalts. The LSLSZ Paleo-Tethys Ocean finally closed in the Triassic.

1. Introduction

As relicts of ancient oceans, ophiolites indicate the occurrence of suture-zone and post-collisional-zone processes, and are therefore useful for investigating the evolution of orogenic belts and for reconstructing tectonic histories (Savov et al., 2001; Xu et al., 2003). Volcanic rock associations preserved in ophiolites generally offer a means of assessing the processes and conditions of basaltic magmatism through time (Ghazi et al., 2012). Therefore, the study of volcanic rocks provides a key for evaluating the evolution of the oceanic lithosphere.

The Longmuco-Shuanghu-Lancang suture zone (LSLSZ), located in central Qiangtang, on the Qinhai-Tibet Plateau, extends for at least 1000 km from western Longmuco to the east of Changdu (Fig. 1a). The LSLSZ is characterized by ophiolitic fragments, high-pressure metamorphic rocks, mélanges, and volcanic rocks, and is interpreted to represent the relicts of the main Paleo-Tethys Ocean basin (Li, 2008; Wu, 2013). However, some scholars have considered that the LSLSZ represents a rifting environment (Wang et al., 1987; Yin, 1997). In addition, Kapp et al. (2003) proposed that the metamorphic rocks were underthrust southward beneath the Qiangtang continental margin during Triassic low-angle oceanic subduction along the Jinsha suture, and that they were then exhumed to upper crustal levels by Late Triassic-Early Jurassic normal faulting. The controversy about the origins of the LSLSZ remains active on account of the paucity of systematic detailed data on LSLSZ ophiolites.

Previous studies of the LSLSZ have focused mainly on the geochemistry and isotopic dating of high pressure (blueschist and eclogite facies) metamorphic rocks (Zhai et al., 2009, 2010; Li et al., 2006, 2009; Dong et al., 2009). Recently, regional geological surveys in Qiangtang have revealed an increasing number of ophiolitic sequences in the region (Zhai et al., 2007; Li, 2008; Wu et al., 2009); these sequences provide important evidences for understanding the tectonic evolution of the LSLSZ.

In this study, we conducted petrological and whole-rock geochemical investigations of the metabasalts from the Taoxinghu ophiolite in the western part of the LSLSZ. The results elucidate the petrogenetic history of the metabasalts and help to constrain the tectonic setting of the Taoxinghu ophiolite, and the evolution history of LSLSZ.

2. Geological setting

Longmuco-Shuanghu-Lancang suture zone is mainly composed of blueschist, eclogite and ophiolite rocks. The blueschist and eclogite occur in Gangmaco, Gemu, Rongma and Shuanghu areas (Zhai et al., 2013) (Fig. 1a), and show subducted E-MORB and OIB affinities, and yield ages of 214-240 Ma (Zhai et al., 2010, 2011; Li et al., 2006, 2009; Pullen et al., 2008; Dong et al., 2009; Zhai et al., 2009). The P-T conditions of the

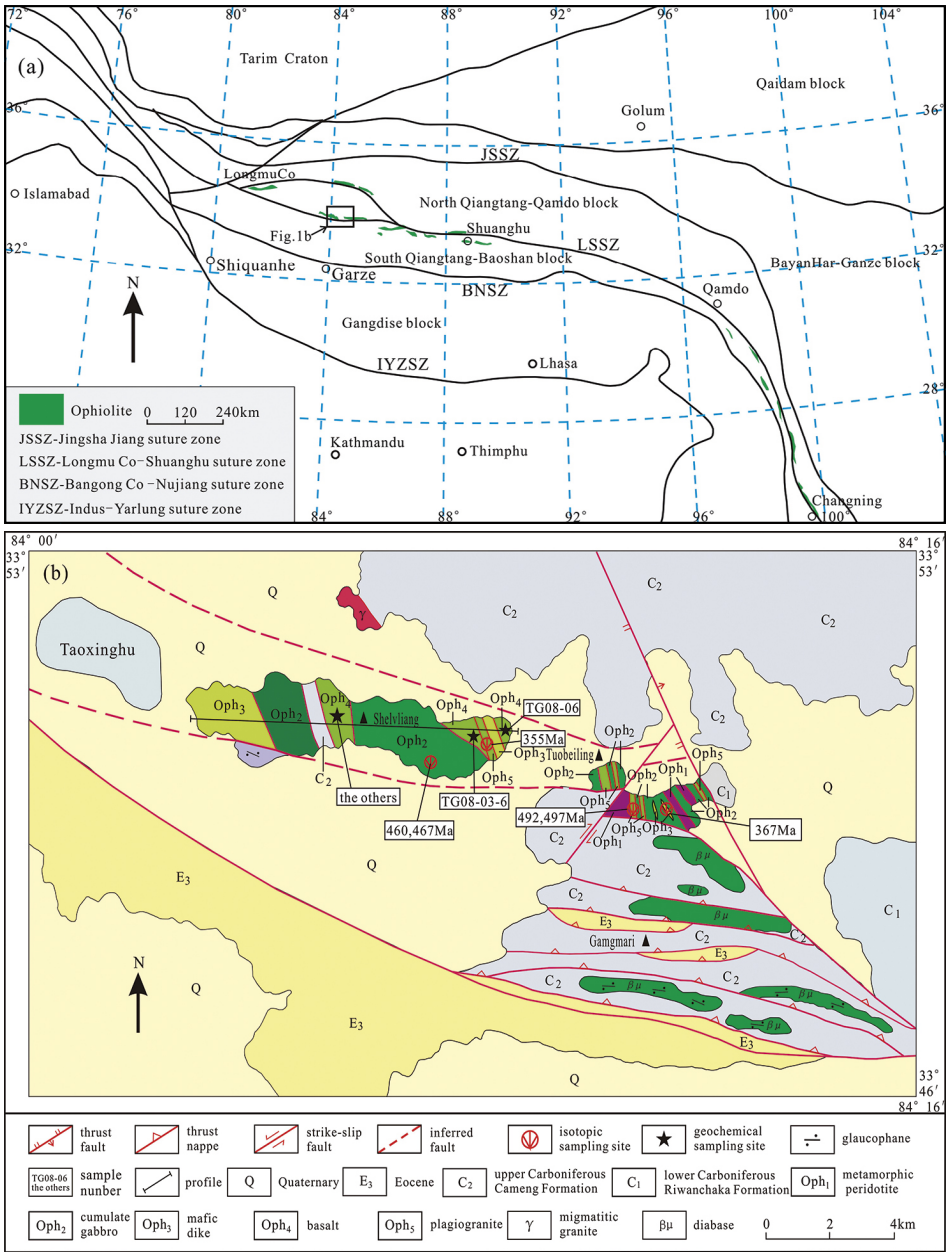

Figure 1b. (a) Map showing tectonic units and the distribution of ophiolite in the Longmuco-Shuanghu-Lancang suture zone, and (b) a schematic geological map of the Taoxinghu ophiolite in central Qiangtang (modified from Wu et al. 2009).

peak eclogite-facies and blueschist-facies metamorphisms are (230-244Ma, Zhai et al., 2011; Pullen et al., 2008) 410-460 °C and 2.0-2.5 GPa (Zhai et al., 2011) and 330-415°C and 9-11.5 kbar (Tang and Zhang 2013), respectively. Recent field mapping shows that the ophiolites from Taoxinghu, Guoganjianan, Gangmaco and Jiaomuri areas in Qiangtang (Li et al. 2008; Wang et al. 2008; Zhai et al. 2010, 2013). However, no complete sequence of ophiolite has been preserved. Cambrian-Permian zircon U-Pb ages have been obtained from metagabbro, metabasalt and plagiogranite of these ophiolites (e.g. Wang et al., 2008; Zhai et al. 2013), implying a long evolution period for Paleo-Tethys Ocean (Wu, 2013). Geochemical analyses of these ophiolites show a progressive evolution from MORB in Cambrian to SSZ in Permian (Wu, 2013).

The Taoxinghu area in the western part of the LSLSZ is located ~200 km north of Gaize, central Qiangtang (Fig. 1a). The structural style of the Taoxinghu area is dominated by E-W-trending faults, and overthrust structures in the Gangmacuo area (Xie et al., 2010). The upper Carboniferous Cameng Group consists of a low-grade metamorphic sequence, consisting of metamorphosed quartz sandstone, schist, phyllite, crystalline limestone, and mafic volcanic rocks, along with glacial diamictite and some mafic volcanic rocks (diabase and basalt) that have undergone blueschist-facies metamorphism (Li, 2003; Geological Survey Academy of Guizhou Province, 2005). The lower Carboniferous Riwanchaka Group consists of limestone and clastic rock containing a Yangtze-type fauna, including coral and brachiopods. Brecciform cataclastic limestone with calcite veins is observed to the east of the ophiolitic mélange, and is inferred to be early Carboniferous in age. Paleogene strata, consisting of red sandstone and conglomerate, occur mainly in the southern part of the study area.

The Taoxinghu ophiolite, ~14 km long and 2-3 km wide, is oriented E-W between Shelvliang and Tuobeiling, where it is divided into the Shelvliang and Tuobeiling ophiolites based on outcrop location (Fig. 1b). Taoxinghu ophiolite is dismembered, and the ophiolitic members occur as block and slice and are in fault contact with each other (Fig. 2). The Shelvliang ophiolite consists mainly of cumulate gabbro, cumulate pyroxenite, gabbro dikes, plagiogranite, and metabasalt (Wu et al., 2009; Zhai et al., 2010). The Tuobeiling ophiolite includes metamorphic peridotite, cumulate gabbro, cumulate pyroxenite, gabbroic dikes, and plagiogranite (Wu et al., 2009; Zhai et al., 2010). These ophiolitic rocks have been variably altered; the peridotites are mostly serpentinized, with the modal content of serpentine varying from 60 % to 80 % (Wu et al., 2013). The cumulate gabbro and gabbro dikes have mostly undergone greenschist- to lower amphibolite-facies

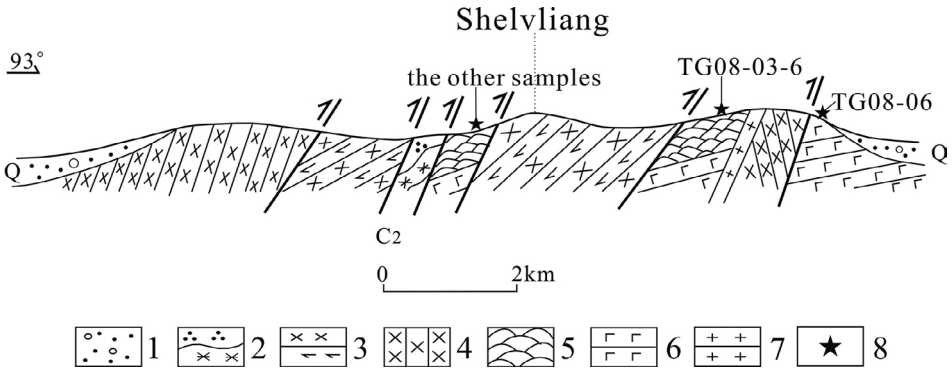

Figure 2. Profile of Shelvliang ophiolite in Chabu town, Gaize country (modified from Wu et al., 2009). 1 – Quaternary sediment; 2 – actinolite quartz schist; 3 – cumulate; 4 – diabase dike; 5 – pillow basalt; 6 – massive basalt; 7 – plagiogranite; 8 –sampling location

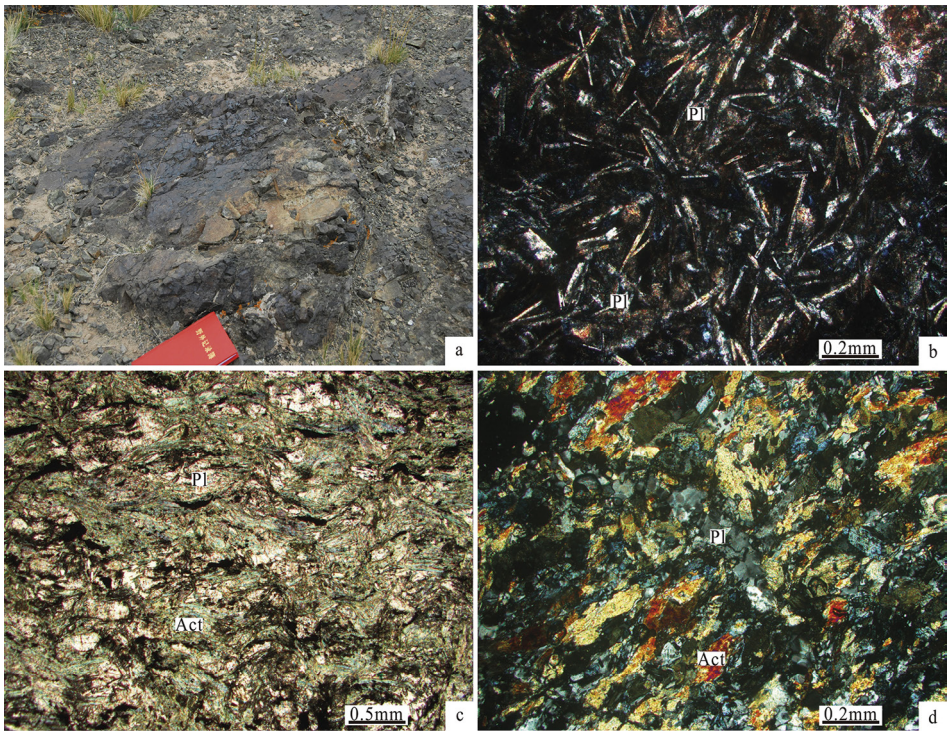

Figure 3. Representative petrographic characteristic of metabasalts from Taoxinghu ophiolite. a-pillow basalt; b-interstitial texture of basalt; c, d-actinolite schist; Pl-plagioclase; Act-actinolite; Zo-zoisite

metamorphism, with pyroxene being replaced by amphibole. Zhai et al. (2010) reported a zircon SHRIMP U-Pb age of 467±4 Ma from these metagabbros, which have similar characteristics to those in the mid-ocean ridge basalts.

3. Petrology

The basalts examined in this study were collected from the Shelvliang ophiolite, and sample locations are shown in Figure 1b and 2. The basalts occur as slices in fault contact with cumulate gabbro, plagiogranite, and Late Carboniferous quartz schist (Fig. 2). The basalts mainly display small to large brecciated pillow structure, with pillows up to 80 cm in diameter (Fig. 3a), and massive basalts are only found in the eastern part of Shelvliang ophiolite (Fig. 2). The fresh basalts mostly show intersertal textures with glass filling the spaces between subhedral crystals of plagioclase (crystal size, 0.2-0.5 mm), and the plagioclase laths show various degree of alteration to clay minerals and sericite (Fig. 3b). Most of the basalts have undergone greenschist-facies metamorphism and contain mineral assemblages of actinolite (50-60 %) and plagioclase (40-50 %), with minor zoisite and epidote (Fig. 3c, d). The metamorphic minerals are often slightly oriented. These metabasalts have similar mineral assemblages to the metagabbro of Taoxinghu ophiolite and metamorphic mafic rocks from other ophiolites in LSLSZ (e.g. Li et al., 2008; Zhai et al., 2010, 2013), suggesting that their metamorphic degree are basically identical.

4. Geochemistry

4.1 Analytical methods

Samples were powdered to less than 200 mesh for whole-rock analyses, performed at the Geological Survey, Hebei Province, Langfang, China. Major element oxide compositions and trace element concentrations were determined on samples TG07 and TG08 at the Chinese Academy of Geological Sciences, Beijing, China. Major element analyses were performed by X-ray fluorescence spectrometry (XRF) and trace element concentrations were determined by inductively coupled plasma-mass spectrometry (ICP-MS), inductively coupled plasma-optical emission spectrometry (ICP-OES), and X-ray fluorescence spectrometry (XRF). Standards GSR2 and GSR3 were used in analyses of both major and trace elements. The analytical precision (relative standard deviation) was generally better than 2 % for major elements and better than 5 % for trace elements. The whole-rock elemental composition of sample Tg10 was determined at the China University of Geoscience, Beijing, China. Major and trace element abundances were determined using a PS-950 XRF and an Agilent 7500a ICP-MS, respectively. Analytical details and results of analyses of reference materials are reported in Yu (2011). The analytical results are listed in Table 1.

Sample	Tg10-23-H1	Tg10-23-H2	Tg10-23-H3	Tg10-23-H4	Tg10-23-H5	Tg10-23-H6	Tg10-23-H7	Tg10-23-H8	Tg10-23-H9	Tg10-23-H10	TG08-01-6	TG08-04-6	T07-18	T07-18R	T07-19	TG08-03-6	TG08-06
SiO_2	54.42	59.40	55.59	58.89	59.16	56.23	53.19	54.54	52.24	51.89	49.16	53.53	48.72	48.70	45.54	49.37	51.59
TiO_2	1.18	1.05	1.24	1.13	1.09	1.12	1.20	1.30	1.34	1.32	1.28	0.91	1.08	1.09	1.11	1.12	3.80
Al_2O_3	14.41	14.29	13.57	12.82	13.35	13.05	14.57	13.69	14.05	13.98	15.15	16.84	15.04	15.01	15.38	13.79	8.18
Fe_2O_3T	9.99	7.59	9.26	7.89	8.36	9.73	9.23	9.84	9.42	10.58	10.24	9.15	10.56	10.47	10.15	11.72	12.40
MnO	0.13	0.10	0.14	0.12	0.12	0.14	0.13	0.14	0.13	0.15	0.14	0.16	0.21	0.21	0.16	0.21	0.14
MgO	5.80	4.25	5.35	4.58	5.02	5.69	5.43	5.95	5.52	7.18	6.42	5.46	6.82	6.84	6.32	7.94	8.69
CaO	7.28	4.56	8.27	8.22	4.56	6.99	9.24	6.42	10.55	7.12	8.75	8.60	9.33	9.33	11.60	11.67	6.87
Na_2O	3.78	4.08	3.01	2.71	3.78	3.01	2.87	3.26	3.44	3.46	3.36	2.85	3.31	3.31	2.19	2.21	3.81
K_2O	0.04	1.35	0.11	0.18	0.96	0.15	0.48	0.33	0.10	0.28	0.23	0.44	0.25	0.25	0.59	0.04	1.43
P_2O_5	0.21	0.23	0.23	0.22	0.21	0.20	0.21	0.24	0.24	0.24	0.22	0.17	0.14	0.14	0.14	0.09	0.44
LOI	2.41	2.42	2.79	2.57	2.62	3.11	3.27	3.81	2.84	3.84	4.40	1.28	4.23	4.26	6.36	1.50	2.08
Total	99.64	99.31	99.55	99.33	99.23	99.42	99.82	99.53	99.86	100.03	99.35	99.39	99.69	99.61	99.54	99.66	99.43
Li	22.48	22.30	23.68	22.10	25.17	28.86	27.24	26.02	20.94	27.62	31.50	5.77	–	–	–	9.28	32.60
Be	–	–	–	–	–	–	–	–	–	–	0.63	0.92	–	–	–	0.24	2.17
Sc	31.22	26.64	32.34	33.64	27.25	32.08	32.96	33.78	34.76	34.02	30.50	22.90	37.50	38.30	38.60	48.50	30.90
V	242	196	236	253	206	236	280	233	281	261	244	223	257	261	270	311	309
Cr	149	109	145	174	127	165	159	173	493	197	172	92	219	216	198	101	558
Co	32.64	24.42	32.22	34.54	26.20	35.60	31.08	35.70	36.08	42.40	40.50	29.90	40.80	41.20	41.60	45.70	51.80
Ni	93.94	68.66	87.36	110	76.31	108	97.56	113	425	131	119	57.80	103	103	89.50	60.30	307
Mn	945	749	981	1044	869	1074	1011	1065	1137	1366	–	–	–	–	–	–	–
Cu	51.01	42.84	57.81	77.62	47.82	72.30	63.25	64.43	72.73	82.37	72.50	49.60	87.20	88.40	105	40.70	153
Zn	52.62	62.00	70.49	83.23	78.83	107	86.92	86.50	68.77	101	91.20	94.60	87.10	87.50	87.90	120	139
Ga	16.91	15.27	16.25	17.35	15.19	17.39	20.26	16.21	19.50	18.13	20.50	20.50	16.20	16.50	17.50	18.40	21.60
Ge	–	–	–	–	–	–	–	–	–	–	0.95	1.08	1.96	1.97	1.69	0.99	0.69
Cs	0.78	3.45	1.62	1.70	2.51	2.46	8.25	4.44	1.18	5.03	2.75	0.43	0.31	0.32	0.49	0.28	1.45
Rb	1.34	40.52	4.17	7.12	28.34	7.91	29.62	15.37	3.70	11.69	10.90	4.11	7.62	7.68	17.90	0.79	42.20
Ba	40.20	538	97.18	77.98	379	145	169	161	30.53	203	72.60	143	62.80	63.00	131	7.04	471
Th	0.72	4.36	0.88	0.88	5.21	0.76	0.84	0.94	0.69	0.68	0.77	0.65	2.77	2.84	2.91	0.11	8.09
U	0.19	1.05	0.21	0.23	1.08	0.19	0.20	0.23	0.20	0.15	0.20	0.10	0.65	0.64	0.62	0.19	2.08
Nb	4.67	7.97	5.52	6.05	7.94	5.14	5.16	5.91	5.93	5.48	4.27	2.79	9.13	9.34	9.73	0.92	49.20
Ta	0.31	0.60	0.35	0.39	0.63	0.33	0.34	0.39	0.38	0.36	0.29	0.19	0.61	0.61	0.62	0.11	3.57
La	8.99	17.81	9.64	10.63	16.82	8.28	8.96	10.40	9.23	8.76	7.04	11.00	11.20	11.60	11.70	1.77	48.90
Ce	20.80	38.52	22.92	24.92	37.56	19.96	21.58	24.48	20.55	19.45	17.10	26.80	23.40	24.40	24.50	6.05	104
Pb	1.08	12.34	1.65	2.83	7.82	1.49	1.86	2.42	1.09	1.61	1.64	4.77	4.10	4.12	6.24	0.72	6.13
Pr	2.87	4.87	3.17	3.43	4.70	2.78	3.01	3.37	2.94	2.78	2.45	3.48	2.90	3.04	3.14	1.09	12.80
Sr	180	381	185	310	398	205	286	365	144	271	312	519	161	164	422	103	306
Nd	13.86	20.74	15.18	16.41	19.88	13.43	14.48	16.05	14.05	13.27	11.90	15.30	12.90	13.50	14.20	6.51	51.80
Zr	86.00	126	94.28	104	134	84.85	87.27	101	95.10	91.44	77.50	37.30	88.60	89.30	92.80	55.40	320
Hf	2.08	3.15	2.36	2.58	3.38	2.11	2.20	2.52	2.25	2.25	2.21	1.33	2.30	2.31	2.40	1.73	8.45
Sm	3.84	4.89	4.21	4.59	4.73	3.78	4.10	4.42	3.83	3.60	3.28	3.27	3.23	3.37	3.52	2.44	10.20
Eu	1.30	1.35	1.39	1.48	1.25	1.23	1.33	1.48	1.32	1.24	1.24	1.02	1.02	1.05	1.16	1.00	3.14
Ti	8157	7288	8829	9348	7626	8516	8799	9008	9454	9366	7672	5455	6474	6533	6653	6713	22777
Gd	4.51	5.06	4.90	5.34	4.89	4.45	4.81	5.19	4.47	4.23	4.31	3.46	3.68	3.73	4.01	3.98	9.14
Tb	0.72	0.77	0.78	0.86	0.75	0.72	0.77	0.84	0.75	0.71	0.69	0.51	0.65	0.65	0.69	0.69	1.24
Dy	4.63	4.90	5.03	5.52	4.77	4.57	4.92	5.36	4.62	4.33	4.57	3.17	4.06	4.13	4.31	5.05	6.71
Y	25.72	27.28	27.70	30.82	26.68	25.32	27.56	29.78	25.75	24.42	23.50	15.70	23.50	23.60	24.80	28.10	26.90
Ho	0.93	0.97	1.01	1.11	0.95	0.91	0.99	1.08	0.95	0.90	0.96	0.63	0.89	0.89	0.94	1.13	1.16
Er	2.69	2.83	2.92	3.21	2.78	2.65	2.84	3.13	2.76	2.61	2.70	1.82	2.41	2.46	2.55	3.20	2.90
Tm	0.42	0.45	0.46	0.51	0.44	0.41	0.44	0.49	0.41	0.39	0.37	0.25	0.37	0.37	0.38	0.47	0.36
Yb	2.51	2.70	2.74	3.02	2.64	2.46	2.62	2.94	2.47	2.35	2.47	1.71	2.37	2.35	2.45	3.17	2.03
Lu	0.37	0.40	0.41	0.44	0.39	0.37	0.38	0.43	0.36	0.35	0.36	0.27	0.35	0.35	0.36	0.45	0.28
$Mg^{\#}$	57.49	56.63	57.41	57.51	58.32	57.66	57.83	58.48	57.71	61.26	59.37	58.18	60.08	60.36	59.20	61.22	62.03
Eu/Eu*	0.95	0.83	0.94	0.91	0.79	0.92	0.92	0.95	0.98	0.97	1.01	0.93	0.90	0.91	0.94	0.98	0.99
∑REE	68.44	106.26	74.77	81.47	102.56	66.00	71.22	79.67	68.72	64.97	59.44	72.69	69.43	71.89	73.91	37.00	254.66
$(La/Yb)_N$	2.57	4.73	2.52	2.52	4.57	2.41	2.45	2.54	2.68	2.68	2.04	4.61	3.39	3.54	3.43	0.40	17.28
$(La/Sm)_N$	1.51	2.35	1.48	1.50	2.30	1.41	1.41	1.52	1.56	1.57	1.39	2.17	2.24	2.22	2.15	0.47	3.09
Ce/Zr	0.24	0.31	0.24	0.24	0.28	0.24	0.25	0.24	0.22	0.21	0.22	0.72	0.26	0.27	0.26	0.11	0.33
Ti/Y	317	267	319	303	286	336	319	302	367	384	326	347	275	277	268	239	847
Th/Yb	0.29	1.62	0.32	0.29	1.97	0.31	0.32	0.32	0.28	0.29	0.31	0.38	1.17	1.21	1.19	0.03	3.99
Th/Nb	0.15	0.55	0.16	0.15	0.66	0.15	0.16	0.16	0.12	0.12	0.18	0.23	0.30	0.30	0.30	0.12	0.16
Zr/Nb	18.4	15.8	17.1	17.1	16.8	16.5	16.9	17.1	16.0	16.7	18.1	13.4	9.70	9.56	9.54	60.2	6.50
Nb/Yb	1.86	2.95	2.02	2.00	3.01	2.09	1.97	2.01	2.40	2.33	1.73	1.63	3.85	3.97	3.97	0.29	24.2
Dy/Yb	1.84	1.81	1.83	1.83	1.81	1.85	1.88	1.82	1.87	1.84	1.85	1.85	1.71	1.76	1.76	1.59	3.31
La/Yb	3.59	6.60	3.52	3.52	6.38	3.36	3.42	3.54	3.74	3.73	2.85	6.43	4.73	4.94	4.78	0.56	24.1
Sr/Nd	13.0	18.4	12.2	18.9	20.0	15.2	19.8	22.8	10.3	20.4	26.2	33.9	12.5	12.1	29.7	15.8	5.91

$Mg^{\#}=100\times Mg^{2+}/(Mg^{2+}+Fe^{2+})$; $Eu/Eu^{*}=Eu_N/SQRT(Sm_N\times Gd)$

Table 1 The concentration of major (wt. %), trace elements (ppm) and their parameters for metabasalts from Taoxinghu ophiolite.

4.2 Metamorphism and elemental mobility

Generally, major elements abundances of metamorphic rocks are inherited from the original protoliths. However, different elements exhibit different behaviors in relation to the degree of alteration and metamorphism. Some elements are relatively mobile, whereas others are relatively immobile (Guilmette et al., 2009). For example, K, Na, Si, and Ca are mobile under conditions of greenschist- and amphibolite-facies metamorphism, while Ti, Al, Mn, and P are relatively stable and Zr, Sc, and Y are very immobile under such conditions (Ghazi et al., 2012; Coish, 1977; Winchester and Floyd, 1977; Pearce and Cann, 1973). In addition, some researchers have suggested that elements with high ionic potential (e.g., K, Ba, Sr, Cs, and Rb) are mobile, while Ta, Nb, trace elements (Cr, Co, Ni, V), and REEs are stable during greenschist- and amphibolite-facies metamorphism (Mullen, 1983; Seewald et al., 1990). Petrological characteristics show that the analyzed samples of the present study experienced greenschist-facies metamorphism. Therefore, when using whole-rock geochemical data of metamorphic rocks to infer the nature and origin of rock units samples, we selected relatively immobile element concentrations and related discrimination diagrams for analysis.

4.3 Geochemistry of the Taoxinghu metabasalts

4.3.1 Major elements

Results of 17 whole-rock geochemical analyses of metamorphic basalt samples are shown in Table 1. Analyses of 16 of the samples show SiO_2 concentrations of 45.54-59.40 wt.%, Al_2O_3 concentrations of 8.18-16.84 wt.%, CaO concentrations of 4.56-11.67 wt.%, MgO concentrations of 4.25-8.69 wt.% (Table 1), and a total alkali content (Na_2O + K_2O) of 2.23-5.51 wt.%. Concentrations of TiO_2 are 0.91-1.34 wt.% (except for sample TG08-06), which are similar to those of basalts from back-arc basins (0.7-2 wt.%, Pearce and Peate, 1995; Gribble et al., 1996, 1998; Leat et al., 2000; Fretzdorff et al., 2002; Sinton et al., 2003). Concentrations of MnO and P_2O_5 are less than 0.5 wt.%, and loss on ignition (LOI) values are 1.28-6.36 wt.%. The $Mg^{\#}$ values (56-62) are less than those of primary magma (68-75, Wilson, 1989), suggesting a low degree of crystal differentiation (Table 1). We classified the rocks based on concentrations of P_2O_5, MgO, Zr, Ti, Nb, and Y. According to the Zr/Ti vs. Nb/Y rock classification diagram of Winchester and Floyd (1977), the analyzed samples range from basaltic to andesitic, and lie close to the subalkaline rock series (except for sample TG08-06, which is an alkaline basalt) (Fig. 4a). The Zr-P_2O_5 diagram (Fig. 4b) shows that one sample plot as alkaline basalts and the others fall into the tholeiitic field.

4.3.2 REEs and trace elements

The 17 samples exhibit different rare earth and trace elements distribution patterns (Fig. 5a, b). Fifteen samples show REE distributions similar to cause of formation. Values of ΣREE are from 59.44 ppm to 106.26 ppm, with mean of 70.06 ppm; the ratio of light REE to heavy REE (LREE/HREE) is 2.62-5.25, with a mean of 3.65; HREE contents are very low (e.g., the Yb content is from 1.71 ppm to 3.02 ppm), suggesting that garnet is present in magma source residues. Chondrite-normalized REE distributions show LREE enrichment, with a negative (right-leaning) slope (Fig. 5a); differentiation of LREEs and HREEs is relatively weak; La_N/Yb_N values are 1.93-4.46, with a mean of 3.08, and there are no obvious Eu or Ce anomalies; Eu/Eu* values are 0.79-1.01, with a mean of 0.92, indicating that plagioclase has not separated or crystallized from the melt. The REE distribution curves are generally parallel, and means for each sample show that the REEs are derived from a cognate magma. Primitive-mantle-normalized trace element

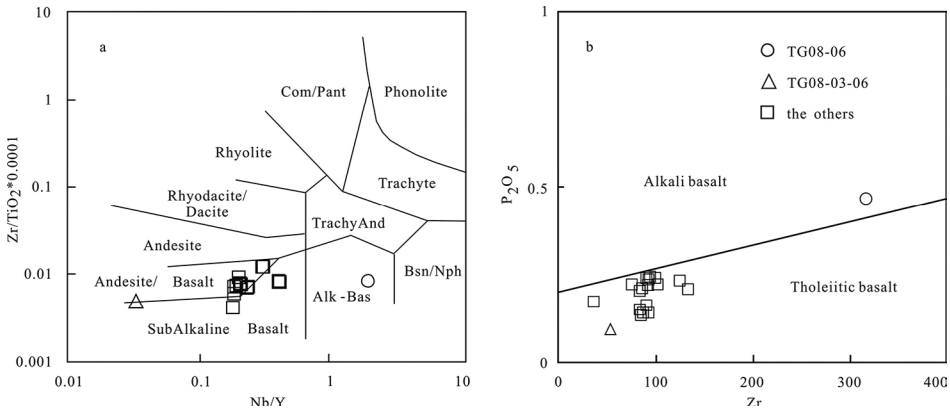

Figure 4. Geochemical classifications for the metabasalts. (a) Diagram of Zr/(TiO_2×0.0001) versus Nb/Y (after Winchester and Floyd, 1977). (b) Plot of Zr versus P_2O_5. The boundary line between tholeiitic and calc-alkaline rock types is from Miyashiro (1974).

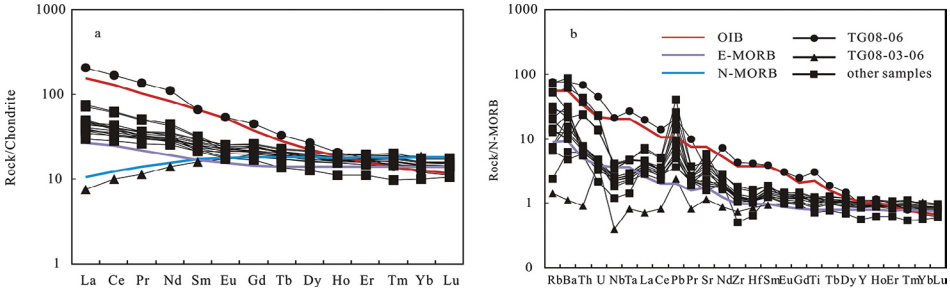

Figure 5. Chondrite-normalized REE diagrams (a) and N-MORB-normalized spider diagrams (b) for metabasalts (normalizing values are from Sun and McDonough, 1989).

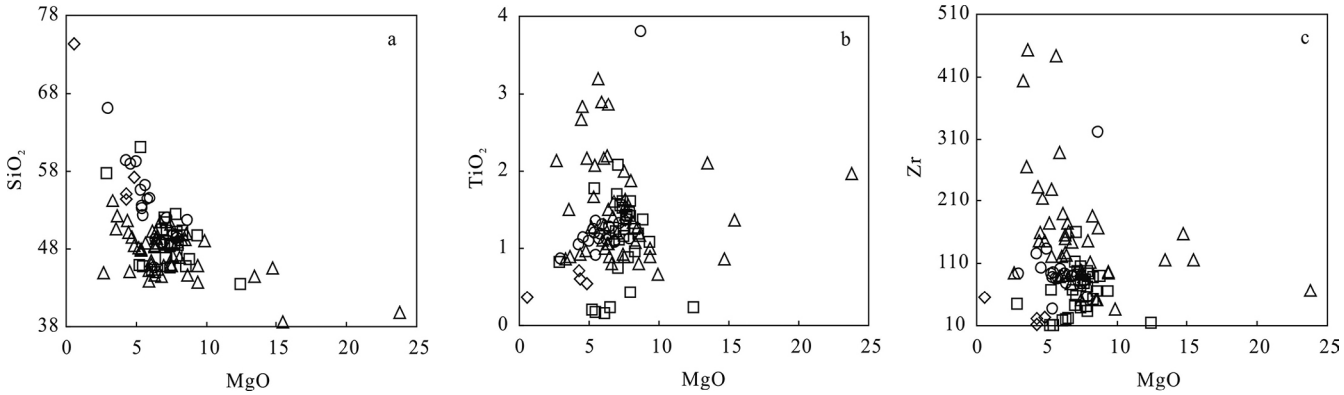

Figure 6. Mafic rocks from LSLSZ ophiolites plotted in the Bowen diagrams for SiO_2, TiO_2 and Zr. The legend is shown in Figure 7.

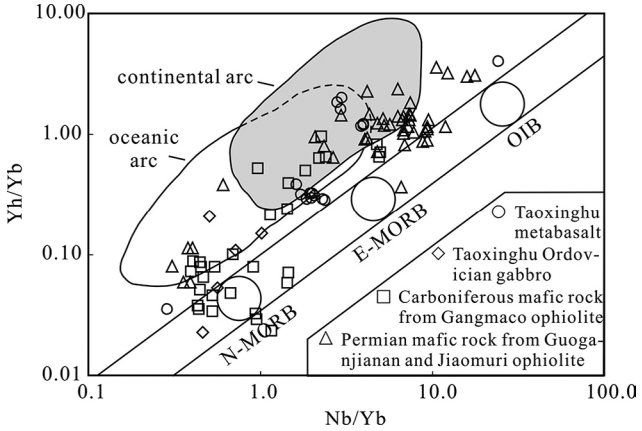

Figure 7. Th/Yb versus Nb/Yb diagram for mafic rocks from LSLSZ ophiolites (after Pearce and Peate, 1995). The geochemical data are from the following sources: Taoxinghu Ordovician gabbro (Zhai et al., 2010); Carboniferous mafic rock from Ganmaco ophiolite (Zhai et al., 2013); Permian mafic rock from Guoganjianan and Jiaomuri ophioltie (Zhai et al., 2006)

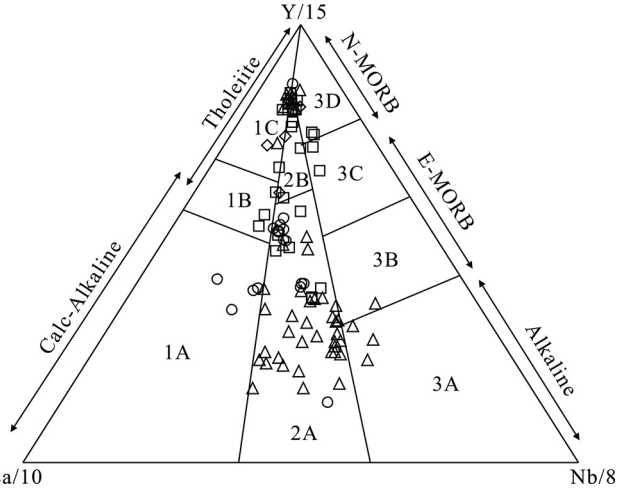

Figure 8. Ternary Y/15-La/10-Nb/8 diagram of Cabanis and Lecolle (1989). 1A, calc-alkaline basalts; 1B, overlap between 1A and 1C; 1C, volcanic arc tholeiites; 2A, continental basalts; 2B, back arc basin basalts; 3A, alkaline basalts; 3B and C, E-MORB; 3D, N-MORB. The legend is shown in Fig.7.

distributions are enriched in Rb, Th, K, Pb, and other elements, and show negative Nb, Ta, and Ti anomalies; normalized REE and trace element distribution patterns are similar to those of island arc basalts (Fig. 5b).

In sample TG08-03-06, the ΣREE content is 37 ppm, the LREE/HREE ratio is 1.04, the La_N/Yb_N ratio is 0.38, the Eu/Eu* value is 0.98, and the Ce/Ce* value is 0.99, indicating no clear fractionation between LREEs and HREEs. Chondrite-normalized REE distributions show depletion in LREEs and almost no Eu or Ce anomalies. Figure 5a shows a depletion in LREEs and flat distributions of HREEs, which are similar to normal mid-ocean ridge basalt (N-MORB)-type REE distributions (Sun and McDonough, 1989). Figure 5b shows that trace elements distributions in the samples are similar to those of N-MORBs. However, compared with N-MORBs, the U, K, and Pb contents of the samples show different degrees of enrichment, wide ranges of variation, and higher concentrations relative to other elements; these differences may be related to the strong activities of these elements or the influence of different degrees of seawater metasomatism. The contents of Nb and Ta show no depletion relative to that of Th, suggesting that the rocks did not form in an island arc setting. Values of Ce/Zr, Zr/Nb, Th/Yb, Zr/Y, Ti/Y, and $(La/Sm)_N$ (0.11, 60.22, 0.03, 1.97, 238.91, and 0.46, respectively) are similar to those of N-MORBs (0.1, 31.76, 0.04, 2.64, 254, and 0.61, respectively) (Sun and McDonough, 1989).

In sample TG08-06 the ΣREE value is 254.66 ppm, the LREE/HREE ratio is 9.69, the La_N/Yb_N ratio is 16.28, the Eu/Eu* values is 0.98, the Ce/Ce* value is 0.96, and total REE, LREE, and HREE contents are relatively high and show clear differentiation; virtually no Eu or Ce anomalies are observed. Chondrite-normalized REE diagrams show LREE enrichment and a flat HREE distribution curve for heavier elements (Fig 5a). A primitive-mantle-normalized incompatible element distribution diagram shows strong high field strength element (HFSE) differentiation of the "big bump" type (Fig. 5b), similar to that of typical OIB distributions.

5. Discussion

5.1 Comparison with mafic rocks from other LSLSZ ophiolites

This section compares the Taoxinghu metabasalt with Taoxinghu metagabbro and then with mafic rocks from other LSLSZ ophiolites.

In which section it was mentionned, Taoxinghu metabasalt show a MORB-IAT geochemical characteristic, similar to suprasubduction-zone (SSZ) ophiolite defined by Dilek and Furnes (2011). This characteristic is rather different from that of Taoxinghu metagabbro, which have N-MORB affinities with LREE depleted REE patterns and negative anomalies in Nb-Ta and Ti (Zhai et al., 2010) (Fig. 5a and b). Bowen diagrams also show no relationship between Taoxinghu metabasalt and metagabbro (Fig. 6). However, in the MgO-TiO_2 and MgO-Zr diagrams, the metabasalts closely match Carboniferous and Permian mafic rocks from Guoganjianan, Gangmaco and Gemu ophiolites, which were formed on subduction zone (Zhai et al., 2013; Wu et al., 2014) (Fig. 6b and c).

The geochemical similarity of Taoxinghu metabasalt and Carboniferous and Permian mafic rocks is also well demonstrated in the Nb/Yb-Th/Yb diagram (Fig. 7). The MORB and OIB domains form a diagonal mantle array on this discriminant diagram, whereas magmas that have interacted with continental crust or have a subduction component are displaced to higher Th/Yb values (Pearce, 2008). Taoxinghu metabasalts closely occupy the space between Carboniferous and Permian mafic rocks, and mostly plot between the MORB array and compositional field for typical arc basalts and in continental arc field. Taoxinghu metabasalts have higher Th/Yb ratios than Carboniferous mafic rocks, showing a stronger subduction-derived component influence. Compared to Permian mafic rocks, Taoxinghu metabasalts are closer to N-MORB, implying their mantle source is more depleted. On the triangular Y-La-Nb diagram, Carboniferous mafic rocks mainly have tholeiite composition and plot in the MORB and back-arc basin basalt fields, whereas Taoxinghu metabasalts and Permian mafic rocks display calc-alkaline character and are rather confined to the area represented by continental arc (Fig. 8). However, most of Taoxinghu metabasalts are closer to back-arc basin basalt field (Fig. 8). These suggest a progressive evolution of LSLSZ ophiolites from MORB to IAT.

Dilek and Furnes (2011) showed that suprasubduction-zone ophiolites may evolve in extending, embryonic backarc to forearc environments, forearc settings, and both oceanic and continental backarc basins. So far, no boninites has been discovered in LSLSZ. Moreover, the hybrid mixture between MORB-like and arc-like element signatures in Taoxinghu metabasalts is generally acknowledged to be unique to back-arc basin basalt (Volpe et al., 1987; Pearce and Peate, 1995; Pearce and Stern, 2006). Taoxinghu metabasalts mostly show E-MORB typed REE patterns (Fig. 5a), and mainly plot closer to the field of for continental arc basalts than to oceanic arc basalts on tectonic discrimination diagrams (Fig. 7 and 8). These characteristics are similar to that of basalt from Okinawa back arc basin (Shinjo et al., 1999). Therefore, the metabasalts from the Taoxinghu ophiolites were probably formed in a continental back-arc and continental arc tectonic setting.

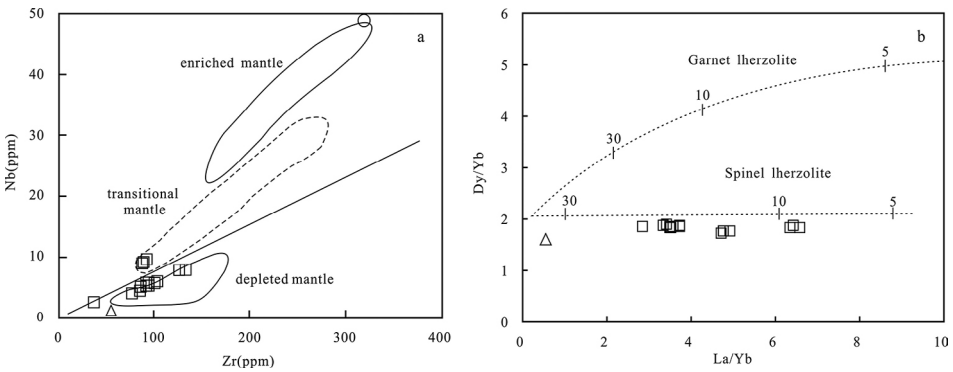

Figure 9. Zr-Nb diagram (a) (Geng et al. 2011) and Dy/Yb-La/Yb diagram (b) (Xu et al. 2001) for Taoxinghu metabasalt. The melting model, mode and partition coefficients are after Xu et al. (2001). Numbers along lines represent the degree of the partial melting.

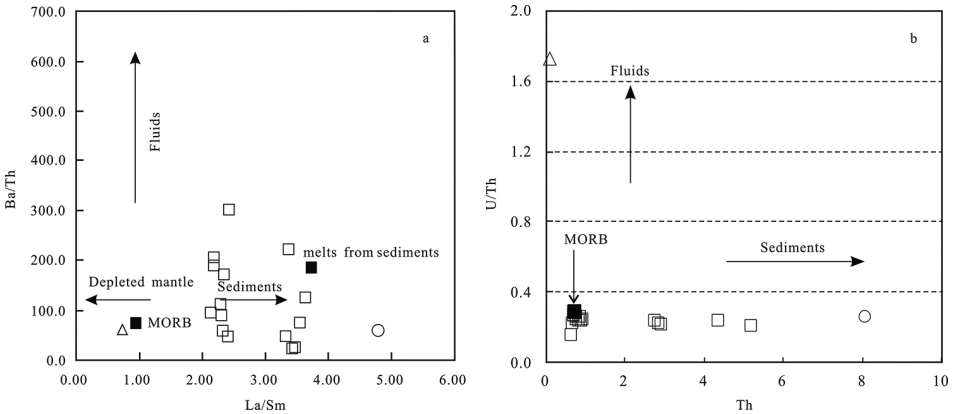

Figure 10. Incompatible element discrimination diagrams for the Taoxinghu metabasalt. (a) Ba/Th-La/Sm diagram (modified after Elliott, 2003); and (b) U/Th-Th diagram (Dilek et al., 2008). The compositions of mid-ocean ridge basalts (MORBs) and magmas resulting from melting of IBMs are given for reference (Hofmann, 1988; Hochstaedter et al., 2001).

5.2 Petrogenesis of the metabasalt

Of the 17 samples, 16 are selectively enriched in large ion lithophile elements (LILEs) and LREEs, and depleted in Nb, Ta, Ti, and HFSEs (Fig. 5b), and 15 samples (all except TG08-03-6 and TG08-06) show relatively high La/Nb ratios (2.9-7.8), Ba/Nb ratios (28.9-134.4), Ba/La (5.2-35.4) ratios, Ba/Th ratios (38-329.3), and Zr/Nb ratios (31.4-79.2), and relatively low Th/Yb ratios (0.1-1). The analyzed samples show that the contents and ratios of elements are similar to those of subduction zone-related rocks (Stern,

2002; Zhou et al., 2004). Generally, such geochemical characteristics are attributed to an enriched mantle with a low degree of partial melting, or the reaction of depleted upper mantle with a mantle plume source, or are influenced by dehydration and release of molten materials during subduction processes (Shilling et al., 1983; Donnelly et al., 2004). However, the 16 samples (all except TG08-06) are depleted in Nb and Ta, showing that the above characteristics are unrelated to the addition of material from a mantle plume source; their TiO_2 concentrations of 0.87%-1.32%, which are lower than the concentrations of a mantle plume source magma, also confirm this. In addition, analyzed samples with high Ba/La and Th/Zr ratios provide evidence for the influence of the fluid component of a subducting plate. Therefore, the enrichment of elements in the Taoxinghu metabasalt and their corresponding ratios may represent contamination by fluids or melting of subducted sediments, or replacement losses caused by the mantle source region.

Elements that are usually inactive (e.g., Zr, Nb, and Yb) were used to identify the characteristics of the magma source (Pearce and Cann, 1973). Except for sample TG08-06, which shows high Nb and Zr contents, the remaining 16 samples show low Nb contents as compared with those of Zr, and show the characteristics of a depleted mantle source (Fig. 9a). Sample TG08-06 has a very high La/Yb ratio (24.1). The La/Yb ratio of TG08-03-6, in contrast, is less than 0.56, and for the remaining 15 samples the La/Yb ratio shows relatively small variations, and, along with high La/Yb ratios (2.85-6.60), show particularly low Dy/Yb ratios (1.52-2.01) (Table 1). On a Dy/Yb-La/Yb diagram (Fig. 9b), the La/Yb value of sample TG08-06 falls outside the scope of the graph, which prevents further analysis of the extent of partial melting of primitive mantle. The diagram shows the remaining 16 samples in the depleted spinel mantle source region, although sample TG08-03-6 may be a spinel lherzolite which is a product of over 30% partial melting of a primitive mantle source. The remaining 15 samples are concentrated near the melting curve representing a spinel mantle source region, or the equivalent of a spinel lherzolite product representing ~6%-25% partial melting of a primitive mantle source.

Previous research has shown that high Ba/Th and low La/Sm ratios are indicative of a mantle source altered by oceanic crustal fluids, and that low Ba/Th ratios are attributed to the melting of sediments (Elliott, 2003). High U/Th ratios are characteristic of a mantle source region that has been influenced by aqueous fluids (Dilek et al., 2008). Therefore, the Ba/Th-La/Sm and U/Th-Th diagrams can be used to consider the influence of aqueous fluids and the contribution of subduction zone materials on the magma source (Fig. 10a and b). With the exception of sample TG08-03-6, the remaining 16 samples reflect the influence of melted sediments, while the influence of aqueous fluids appears to be minimal.

5.3 Implications for the evolution of the Paleo-Tethys in central Qiangtang

Based on an integration of geochemical data and paleontological and radiometric ages from ophiolites along the whole LSLSZ, as well as related paleomagnetic data and geochemical data of volcanic rocks, we propose a geodynamic model for the evolution of the Paleo-Tethys Ocean in central Qiangtang.

The Taoxinghu ophiolite plagioclase granite yields zircon U-Pb ages of 497 and 492 Ma(Hu et al., 2014a). The ophiolite represents the products of partial melting of young oceanic crust. Cumulate gabbros yield a zircon U-Pb age of 467 Ma, and they have MORB-type geochemical characteristics (Zhai et al., 2010). The Guoganjianan ophiolite (240 km east of Taoxinghu) yields zircon U-Pb ages of 438, 431, and 451 Ma (Li et al., 2008; Wang et al., 2008), and it has geochemical MORB-type signatures (Zhai et al., 2007). In eastern Tibet along the eastern edge of the Longmuco-Shuanghu-Lancang suture zone, gabbro and cumulate gabbro ophiolites yield zircon U-Pb ages of 470, 439, and 454 Ma (Wang et al., 2013). These suggest that the Paleo-Tethys Ocean basin may have started to form during the Cambrian or earlier.

Paleomagnetic data from eastern Tibet-western Yunnan show that drift of the Baoshan terrane to the south and of the Yangtze terrane to the north began in the Late Ordovician (ca. 450 Ma), and that separation of the Baoshan and Yangtze terranes may have started in the early Silurian in the western Yunnan area of eastern Tibet, during early rifting of the Paleo-Tethys Ocean basin (Li, 2003).

Initial rifting of the Paleo-Tethys basin occurred at least as early as the Early Ordovician, and the record of the Paleo-Tethys in the Longmuco-Shuanghu-Lancang suture zone may extend to before the early Cambrian in middle to western Qiangtang. The Taoxinghu and Guoganjianan ophiolites yield zircon U-Pb ages of 355, 348, and 355 Ma, and geochemical signatures show that the rocks are the products of partial melting of subducted oceanic crustal material (Shi et al., 2009; stay published data). The above studies show that the Paleo-Tethys Ocean may have subducted in the early Carboniferous. Taoxinghu metabasalts mainly show geochemical characteristics of back-arc basin lavas, implying that a back-arc basin formed during subduction of Paleo-Tethys Ocean.

Results of paleomagnetic analyses show that accretion of the Baoshan and Yangtze blocks started in the early Carboniferous in the area of eastern Tibet to western Yunnan (Li, 2003). Studies on a high-pressure metamorphic belt, exposed in the southern part of the Longmuco-Shuanghu ophiolite belt and extending over 500 km, have shown that the belt formed during 240-214 Ma (Li et al., 2006, 2009; Dong et al., 2009; Zhai et al., 2009). In addition, angular unconformities at the upper contact of the Guoganjianan ophiolite show that the Longmuco-Shuanghu-Lancang suture zone closed by the time of the earliest deposition of sedimentary cover; zircon U-Pb ages of the basal rhyolite interlayer of the Wanghuling Group of 214 Ma (Late Triassic) constrain the timing of closure of the basin and the formation of the suture (Li et al., 2007). Recently, paleogeographic research on Triassic lithofacies on the Tibetan Plateau in the northern Qinghai region has confirmed that the Paleo-Tethys Ocean had closed by the begin Triassic in central Qiangtang (Zhu et al., 2013).

In conclusion, the Paleo-Tethys Ocean basin, represented by the Longmuco-Shuanghu-Lancang suture zone, may have started to form during the Cambrian or earlier, and until the early Carboniferous the basin was in a stage of expansion. Starting in the early Carboniferous, however, expansion of the basin ceased and the basin had closed by the begin Triassic in midwest Qiangtang.

6. Conclusions

(1) The Taoxinghu ophiolite metabasalts experienced greenschist-facies metamorphism, and were formed in a continental back-arc basin. The ophiolite represents the first discovery of the upper-level lavas of typical SSZ-type ophiolites in the Longmuco-Shuanghu-Lancang suture zone.

(2) The metabasalts were likely formed from a depleted spinel mantle source region, with a spinel lherzolite content equivalent to 6 %-25 % partial melting; one samples show spinel lherzolite contents equivalent to >30 % partial melting, and one sample shows signatures of enriched mantle. The metabasalts reflect the contributions of melted sediment, while the influence of aqueous fluids may have been minimal.

(3) The LSLSZ Paleo-Tethys Ocean opened during the Cambrian or earlier, and subduction began in the early Carboniferous. As subduction proceeding, a continental back-arc basin developed. The LSLSZ Paleo-Tethys Ocean was closed in the Triassic.

Acknowledgment

We appreciate Prof. Yongsheng Dong for his help during petrography work. We thank research team of Tibet, Jilin University for their assistance with the fieldwork. We also thank reviewers for their comments. Our research is supported by the Postdoctoral Science Foundation of China [No.2014M561023] and the National Natural Science Foundation of China [Nos. 40872146, 41072166, 41272240], the Project of China Geological Survey [No. 1212011086061, 1212011221093, 1212011087009].

References

Cabanis, B. and Lecolle, M., 1989. The La/10-Y/15-Nb/8 diagram: a tool for discrimination volcanic series and evidencing continental crust magmatic mixtures and/or contamination. Compte Rendus de l'Academie des Sciences, Seris II, Mécanique, Physique, Chimie, Sciences de l'univers, Sciences de la Terre, 309, 2023-2029.

Coish, R.A., 1977. Ocean floor metamorphism in the Betts Cove Ophiolite, Newfoundland. Contributions to Mineralogy and Petrology, 60, 277-302. http://dx.doi.org/ 10.1007/BF01166800

Dilek, Y. and Furnes, H., 2011. Ophiolite genesis and global tectonics: Geochemical and tectonic fingerprinting of ancient oceanic lithosphere. Geological Society of America Bulletin, 123, 387-411. http://dx.doi.org/10.1130/B30446.1

Dilek, Y., Furnes, H. and Shallo, M., 2008. Geochemistry of the Jurassic Mirdita Ophiolite (Albania) and the MORB to SSZ evolution of a marginal basin oceanic crust. Lithos, 100, 174-209. http://dx.doi.org/10.1016/j.lithos.2007.06.026

Dong, Y.S., Zhang, X.Z., Shi, J.R. and Wang, S.Y., 2009. Petrology and metamorphism of garnet-muscovite schist from high pressure metamorphic belt in central Qiangtang, northern Tibet. Geological Bulletin of China, 28, 1204-1206. (in Chinese with English abstract)

Donnelly, K.E., Goldstein, S.L., Langmuir, C.H. and Spiegelman, M., 2004. Origin of enriched ocean ridge basalts and implications for mantle dynamics. Earth and Planetary Science Letters, 226, 347-366. http://dx.doi.org/10.1016/j.epsl.2004.07.019

Elliott, T., 2003. Tracers of the slab. In: Eiler, J. (ed.), Inside the Subduction Factory. AGU, Washington, DC, pp. 23-45.

Fretzdorff, S., Livermore, R.A., Devey, C.W., Leat, P.T. and Stoffers, P., 2002. Petrogenesis of the back-arc East Scotia Ridge, South Atlantic Ocean. Journal of Petrology, 43, 1435-1467. http://dx.doi.org/10.1093/petrology/43.8.1435

Geng, H., Sun, M., Yuan, C., Zhao, G., Xiao, W., 2011. Geochemical and geochronological study of early Carboniferous volcanic rocks from the West Junggar: Petrogenesis and tectonic implications. Journal of Asian Earth Sciences, 42, 854-866. http://dx.doi.org/10.1016/j.jseaes.2011.01.006

Geological Survey Academy of Guizhou Province, 2005. 1:250000 Scale Dinggu Regional Geological Survey Report, Unpublished. (in Chinese)

Ghazi, J.M., Moazzen, M., Rahgoshay, M. and Moghadam, H.S., 2012. Geochemical characteristics of basaltic rocks from the Nain ophiolite (Central Iran): Constraints on mantle wedge source evolution in an oceanic back arc basin and a geodynamical model. Tectonophysics, 574-575, 92-104. http://dx.doi.org/10.1016/j.tecto.2011.10.001

Gribble, R.F., Stern, R.J., Bloomer, S.H., Stüben, D., O'Hearn, T. and Newman, S., 1996. MORB mantle and subduction components interact to generate basalts in the southern Mariana Trough back-arc basin. Geochimica et Cosmochimica Acta, 60, 2153-2166. http://dx.doi.org/10.1016/0016-7037(96)00078-6

Gribble, R.F., Stern, R.J., Newman, S., Bloomer, S.H. and O'Hearn, T., 1998. Chemical and isotopic composition of lavas from the Northern Mariana Trough: Implications for magmagenesis in back-arc basins. Journal of Petrology, 39, 125-154. http://dx.doi.org/10.1093/petroj/39.1.125

Guilmette, C., Hébert, R., Wang. C.S. and Villeneuve, M., 2009, Geochemistry and geochronology of the metamorphic sole underlying the Xigaze Ophiolite, Yarlung Zangbo Suture Zone, South Tibet. Lithos, 112, 149-162. http://dx.doi.org/10.1016/j.lithos.2009.05.027

Hochstaedter, A., Gill, J., Peters, R., Broughton, P., Holden, P. and Taylor, B., 2001. Across-arc geochemical trends in the Izu-Bonin arc: contributions from the subducting slab. Geochemistry Geophysics Geosystems, 2, 1019. http://dx.doi.org/10.1029/2000GC000105

Hofmann, A.W., 1988. Chemical differentiation of the Earth: the relationship between mantle, continental crust, and oceanic crust. Earth and Planetary Science Letters, 90, 297-314. http://dx.doi.org/10.1016/0012-821X(88)90132-X

Hu, P.Y., Li, C., Wu, Y.W., Xie, C.M., Wang, M., Li, J., 2014a. Opening of the Longmu Co-Shuanghu-Lancangjiang ocean: constraints from plagiogranites. Chinese Science Bulletin, 59(25): 3188-3199

Kapp, P., Yin, A., Manning, C.E., Harrison, T.M., Taylor, M.H. and Ding, L., 2003. Tectonic evolution of the early Mesozoic blueschist-bearing Qiangtang metamorphic belt, central Tibet. Tectonics, 22, 1043. http://dx.doi.org/10.1029/2002TC001383

Leat, P.T., Livermore, R.A., Millar, I.L. and Pearce, J.A., 2000. Magma supply in back-arc spreading Centre Segment E2, East Scotia Ridge. Journal of Petrology, 41, 845-866. http://dx.doi.org/10.1093/petrology/41.6.845

Li, C., 2003. Question about the Basement of the Qiangtang Micro-Plate. Geolocical Review, 49, 4-9. (in Chinese with English Abstract)

Li, C., 2008. A Review on 20 Years' Study of the Longmu Co-Shuanghu-Lancang River Suture Zone in the Qinghai-Xizang (Tibet) Plateau. Geological Review, 54, 104-119. (in Chinese with English Abstract)

Li, C., Dong, Y. S., Zhai, Q. G., Wang, L. Q., Yan, Q. R., Wu, Y. W. and He, T. T., 2008. Discovery of Eopaleozoic ophiolite in the Qiangtang of Tibet Plateau: Evidence from SHRIMP U-Pb dating and its tectonic implications. Acta Petrologica Sinica, 24, 31-36. (in Chinese with English abstract)

Li, C., Zhai, Q., Dong, Y., Liu, S., Xie, C. and Wu, Y., 2009. High-Pressure Eclogite-Blueschist Metamorphic Belt and Closure of Paleo-Tethys Ocean in Central Qiangtang, Qinghai-Tibet Plateau. Journal of Earth Sciences, 20, 209-218. http://dx.doi.org/10.1007/s12583-009-0021-4

Li, C., Zhai, Q.G., Chen, W., Yan, Q.R., Dong, Y.S. and Yu, J.J., 2007. Geochroology evidence of the closure of Longmu Co-Shuanghu suture, Qinghai-Tibet plateau; Ar-Ar and zircon SHRIMP geochronology from ophiolite and rhyolite in Guoganjiannian. Acta petrologica Sinica, 23, 911-918. (in Chinese with English abstract)

Li, C., Zhai, Q.G., Chen, W., Yu, J.J., Huang, X.P. and Zhang, Y., 2006. Ar-Ar chronometry of the eclogite from central Qiangtang area, Qinghai-Tibet Plateau. Acta Petrologica Sinica, 22, 2843-2849. (in Chinese with English Abstract)

Miyashiro, A., 1974. Volcanic rock series in island arcs and active continental margins. American Journal of Science, 274, 321-355. http://dx.doi.org/10.2475/ajs.274.4.321

Mullen, E.D., 1983, MnO-TiO_2-P_2O_5: a minor element discriminant for basaltic rocks of oceanic environments and its implications for petrogenesis: Earth and Planetary Science Letters, v. 62, p. 53-62.

Pearce, J.A. and Cann, J.R., 1973. Tectonic setting of basic volcanic rocks determined using trace element analyses. Earth and Planetary Science Letters, 19, 290-300. http://dx.doi.org/10.1016/0012-821X(73)90129-5

Pearce, J.A. and Peate, D.W., 1995. Tectonic Implications of the Composition of Volcanic ARC Magmas. Annual Review of Earth and Planetary Sciences, 23, 251-285. http://dx.doi.org/10.1146/annurev.ea.23.050195.001343

Pearce, J.A. and Stern, R.J., 2006. Origin of back-arc basin magmas: Trace element and isotope perspectives. In: D.M. Christie, C.R. Fisher, S.M. Lee and S. Givens (eds.), Back-arc spreading systems: Geological, biological, chemical, and physical interactions. AGU, Washington, DC, pp. 63-86.

Pearce, J.A., 2008. Geochemical fingerprinting of oceanic basalts with applications to ophiolite classification and the search for Archean oceanic crust. Lithos, 100, 14-48. http://dx.doi.org/10.1016/j.lithos.2007.06.016

Pullen, A., Kapp, P., Gehrels, G. E., Vervoort, J. D. and Ding, L., 2008. Triassic continental subduction in central Tibet and Mediterranean-style closure of the Paleo-Tethys Ocean. Geology, 36, 351-354. http://dx.doi.org/10.1130/G24435A.1

Savov, I., Ryan, J., Haydoutov, I. and Schijf, J., 2001. Late Precambrian Balkan-Carpathian ophiolite a slice of the Pan-African ocean crust?: geochemical and tectonic insights from the Tcherni Vrah and Deli Jovan massifs, Bulgaria and Serbia. Journal of Volcanology and Geothermal Research, 110, 299-318. http://dx.doi.org/10.1016/S0377-0273(01)00216-5

Seewald, J.S., Seyfried Jr., W.E., 1990, The effect of temperature on metal mobility in sub seafloor hydrothermal systems: constraints from basalt alteration experiments: Earth and Planetary Science Letters, v. 101, p. 388-403.

Shi, J.R., Dong, Y.S. and Wang, S.Y., 2009. Dating and tectonic significance of plagiogranite from Guoganjianan Mountain, central Qiangtang, northern Tibet, China. Geological Bulletin of China, 28, 1236-1243. (in Chinese with English Abstract)

Shilling, J.G., Zajac, M. and Evans, R., 1983. Petrogolical and geochemical variations along the Mid-Atlantic ridge from 29°N to73°N. American Journal of Sciences, 283, 510-586. http://dx.doi.org/10.2475/ajs.283.6.510

Shinjo, R., Chung, S.L., Kato, Y. and Kimura, M., 1999. Geochemical and Sr-Nd isotopic characteristics of volcanic rocks from the Okinawa Trough and Ryukyu Arc: Implications for the evolution of a young, intracontinental back arc basin. Journal of Geophysical Research: Solid Earth, 104, 10591-10608. http://dx.doi.org/10.1029/1999JB900040

Sinton, J.M., Ford, L.L., Chappell, B. and McCulloch, M.T., 2003. Magma genesis and mantle heterogeneity in the Manus back-arc basin, Papua New Guinea. Journal of Petrology, 44, 159-195. http://dx.doi.org/10.1093/petrology/44.1.159

Stern, R.J., 2002. Subduction zones. Reviews of Geophysics, 40, 1012, http://dx.doi.org/10.1029/2001RG000108

Sun, S.S., and McDonough, W.F., 1989. Chemical and isotopic systematics of oceanic basalts: Implications for mantle composition and processes. Geological Society, London, Special Publications, 42, 313-345. http://dx.doi.org/10.1144/GSL.SP.1989.042.01.19

Tang, X. C. and Zhang, K. J., 2013. Lawsonite- and glaucophane-bearing blueschists from NW Qiangtang, northern Tibet, China: mineralogy, geochemistry, geochronology, and tectonic implications. International Geology Review, 56, 150-166.

http://dx.doi.org/10.1080/00206814.2013.820866

Volpe, A.M., Douglas Macdougall, J. and Hawkins, J.W., 1987. Mariana Trough basalts (MTB): trace element and SrNd isotopic evidence for mixing between MORB-like and arc-like melts. Earth and Planetary Science Letters, 82, 241-254. http://dx.doi.org/10.1016/0012-821X(87)90199-3

Wang, C.S., Hu, C.Z., Wu, R.Z., and Zhang, M.G., 1987. Significance of the discovery of Chasang-chabu rift in northern Xizang (Tibet). Journal of Chengdu College of Geology, 14, 33-47. (in Chinese with English Abstract)

Wang, L.Q., Pan, G.T., Li, C., Dong, Y.S., Zhu, D.C., Yuan, S.H. and Zhu, T.X., 2008. SHRIMP U-Pb zircon dating of Eopaleozoic cumulate in Guoganjianan Mt. from central Qiangtang area of northern Tibet—Considering the evolvement of Proto-and Paleo-Tethys. Geological Bulletion of China, 27, 2045-2056. (in Chinese with English Abstract)

Wang, B.D., Wang, L.Q., Pan, G.T., Yin, F.G., Wang, D.B. and Tang, Y., 2013. U-Pb zircon dating of Early Paleozoic gabbro from the Nantinghe ophiolite in the Changning-Menglian suture zone and its geological implication. Chinese Science Bulletin, 58, 920-930. http://dx.doi.org/10.1007/s11434-012-5481-8

Wilson, M., 1989. Igneous petrogenesis. Springer, London, pp. 245-285.

Winchester, J.A., and Floyd, P.A., 1977. Geochemical discrimination of different magma series and their differentiation products using immobile elements. Chemical Geology, 20, 325-343. http://dx.doi.org/10.1016/0009-2541(77)90057-2

Wu, Y.W., 2013. The evolution record of Longmuco-Shuanghu-Lancang ocean-Cambrian-Permian ophiolites. Doctoral Thesis, Jilin University, Changchun, China. (in Chinese with English Abstract)

Wu, Y.W., Li, C., Dong, Y.S., Xie, C.M. and Hu, P.Y., 2009. Petrological characteristics of Taoxinghu Early Paleozoic ophiolite in central Qiangtang, northern Tibet, China. Geological Bulletin of China, 28, 1290-1296. (in Chinese with English Abstract)

Wu, Y.W., Li, C., Xie, C.M., Wang, M. and Hu, P.Y., 2013. Petrology, geochemistry and tectonic significance of the metamorphic peridotites from Longmuco-Shuanghu Ophiolitic Mélange Belt, Tibet. Acta Geologica Sinica (English Edition), 87, 426-439. http://dx.doi.org/10.3969/j.issn.1000-9515.2013.02.009

Wu, Y.W., Li, C., Xu, M.J., Xie, C.M., Wang, M., Xiong, S.Q. and Fan, Z.G., 2014. Geochemical characteristics and LA-ICP-MS zircon U-Pb geochronology of Guogangjianan Carboniferous ophiolite in central Qiangtang, the Tibetan Plateau. Geological Bulletin of China, 33, 1682-1689. (in Chinese with English abstract).

Xie, C.M., Li, C., Dong, Y.S., Wu, Y.W., Wang, M. and Hu, P.Y., 2010. Gangmari-Juhuashan thrust nappe were discovered in central Qiangtang, northern Tibet, China. Geological Bulletin of China 29, 1857-1862. (in Chinese with English Abstract)

Xu, J.F., Castillo, P.R., Chen, F.R., Niu, H.C., Yu, X.Y. and Zhen, Z.P., 2003. Geochemistry of late Paleozoic mafic igneous rocks from the Kuertiarea, Xinjiang, northwest China: Implications for back arc mantle evolution. Chemical Geology, 193, 137-154. http://dx.doi.org/10.1016/S0009-2541(02)00265-6

Xu, Y.G., Menzies, M.A., Thirlwall, M.F. and Xie, G.H., 2001. Exotic lithosphere mantle beneath the western Yangtze craton: Petrogenetic links to Tibet using highly magnesian ultrapotassic rocks. Geology, 29, 863-866. http://dx.doi.org/10.1130/0091-7613(2001)029<0863:ELMBTW>2.0.CO;2

Yin, J.X., 1997. Stratigraphic Geology of Gondwana Facies of Qinghai-Xizang (Tibet) Plateau and Adjacent Areas. Geological Publishing House, Beijing. (in Chinese with English Abstract)

Yu, H., 2011. Mineral Geochemical Characteristics and Genetic Mechanism of Olivine Rocks in Shangnan, Shanxi. Master Thesis, China University of Geoscience (Beijing), Beijing, China. (in Chinese with English Abstract)

Zhai, Q.G., Jahn, B.M., Wang, J., Su, L., Mo, X.X., Wang, K.L., Tang, S.H. and Lee, H.Y., 2013. The Carboniferous ophiolite in the middle of the Qiangtang terrane, Northern Tibet: SHRIMP U-Pb dating, geochemical and Sr-Nd-Hf isotopic characteristics. Lithos, 168-169, 186-199. http://dx.doi.org/10.1016/j.lithos.2013.02.005

Zhai, Q.G., Li, C. and Huang, X.P., 2006. Geochemistry of Permian basalt in the Jiaomuri area, centr al Qiangtang, Tibet, China, and its tectonic significance. Geological Bulletin of China, 25, 1419-1427. (in Chinese with English Abstract)

Zhai, Q.G., Li, C. and Huang, X.P., 2007. The fragment of Paleo-Tethys ophiolite from central Qiangtang, Tibet: Geochemical evidence of metabasites in Guoganjianan. Science China Earth Sciences, 50, 1302-1309. http://dx.doi.org/10.1007/s11430-007-0051-7

Zhai, Q.G., Li, C. and Wang, J., 2009. Petrology, mineralogy and pTt path for the eclogite from central Qiangtang, northern Tibet, China. Geological Bulletin of China, 28, 1207-1220. (in Chinese with English Abstract)

Zhai, Q.G., Wang, J., Li, C. and Su, L., 2010. SHRIMP U-Pb dating and Hf isotopic analyses of Middle Ordovician meta-cumulate gabbro in central Qiangtang, northern Tibetan Plateau. Science China Earth Sciences, 53, 657-664. http://dx.doi.org/10.1007/s11430-010-0063-6

Zhai, Q.G., Zhang, R.Y., Jahn, B.M., Li, C., Song, S.G. and Wang, J., 2011. Triassic eclogites from central Qiangtang, northern Tibet, China: Petrology, geochronology and metamorphic P-T path. Lithos, 125, 173-189. http://dx.doi.org/10.1016/j.lithos.2011.02.004

Zhou, M., Lesher, M.L. and Yang, Z., 2004. Geochemistry and petrogenesis of 270 Ma Ni-Cu-(PGE) sulfide-bearing mafic intrusions in the Huangshan district, Eastern Xinjiang, Northwest China: Implications for the tectonic evolution of the Central Asian orogenic belt. Chemical Geology, 209, 233-257. http://dx.doi.org/10.1016/j.chemgeo.2004.05.005

Zhu, T.X., Feng, X.T., Wang, X.F. and Zhou, M.K., 2013. Reconstruction of the Triassic Tectonic Lithofacies Paleogeography in Qiangtang Region, Northern Qinghai-Tibet Plateau, China. Acta Geologica Sinica, 87, 378-394. http://dx.doi.org/10.3969/j.issn.1000-9515.2013.02.007

Received: 12 February 2015
Accepted: 22 December 2015

Yan-wang WU[1) 2)], Cai LI[4)], Meng-jing XU[3) *)], Sheng-qing XIONG[1)], Zheng-guo FAN[1)], Chao-ming XIE[4)] & Ming WANG[4)]

[1)] China Aero Geophysical Survey & Remote Sensing Center for Land and Resources, Beijing 100083, China;

[2)] School of Geophysics and Information Technology, China University of Geoscience (Beijing), Beijing 100083, China;

[3)] School of Geology and Geomatics, Tianjin Chengjian University, Tianjin 300384, China;

[4)] College of Earth Science, Jilin University, Changchun 130061, China;

[*)] Corresponding author: mengjing_xu@126.com